Materials Today Communications 35 (2023) 105745

Contents lists available at ScienceDirect

Materials Today Communications

journal homepage: www.elsevier.com/locate/mtcomm

Development of hyaluronic acid-based electroconductive hydrogel as a sensitive non-enzymatic glucose sensor

Didem Aycan, Fatma Karaca, Neslihan Alemdar *

Marmara University, Department of Chemical Engineering, Istanbul, Turkey

ARTICLE INFO

Keywords:
Hyaluronic acid
Reduced graphene oxide
Polyaniline
Electroconductive hydrogel
Glucose sensor

ABSTRACT

Herein, a novel hyaluronic acid (HA)-based electroconductive hydrogel with enhanced mechanical properties was developed for the non-enzymatic glucose detection. As the main component of the polymeric network, HA was modified through methacrylation to integrate photocrosslinkable groups into its backbone. Electrical conductivity was provided to hydrogel by using two different conductivity sources as the introduction of reduced graphene oxide (rGO) and polyaniline (PANI) to HA-based hydrogel structure. The combination of these conductivity sources not only provided the sufficient electrical conductivity (1.58×10^{-5} S/cm) to hydrogels, but also ensured superior mechanical performance in terms of compressive strength (992.1 kPa) and elastic modulus (23.4 kPa) due to the synergistic effect of the rGO and PANI, that are the significant parameters for sensor applications. The electrochemical activity and sensor performance of the HA-based hydrogel were investigated via cyclic voltammetry (CV) and choronoamperometry (CA) methods. The fabricated HA-based hydrogel sensor exhibited high sensitivity as 421.42 $\mu A m M^{-1} cm^{-2}$ and selectivity for glucose with a low detection limit (0.3 μM). Moreover, it showed excellent long-term stability, reproducibility and anti-interference feature towards uric acid, ascorbic acid and sorbitol. Based on these results it could be stated that the developed HA-based hydrogel sensor containing ternary HA-rGO-PANI formulation for the first time in the literature might be served as a promising potential for the non-enzymatic glucose detection and it also offers a new perspective for fabricating efficient hydrogel-based biosensing systems for future studies.

1. Introduction

Recently, hydrogels have gained immense interest in sensor applications due to their highly compatible structure with most biological molecules, and their hydrophilic, biomimetic and tunable nature, which are the crucial requirements for a sensing material [1,2]. Therefore, studies about the production of hydrogel-based sensors have been extensively conducted as an attractive research field [3–7]. To fabricate hydrogel networks through the chemical or physical crosslinking mechanisms, numerous kinds of synthetic (polyvinyl alcohol, polyethylene glycol, polyacrylic acid, polyacrylamide, etc.) and natural-origin polymers (chitosan, chitin, cellulose, hyaluronic acid (HA), alginate, etc.) as a potential substrate for biosensing applications have been explored in latest literature [2,8–11]. Among these polymers, natural-origin polymers emerged as more favorable materials in the fabrication of hydrogel-based sensors than their synthetic kinds because of their outstanding features such as biocompatible, biodegradable, non-toxic, highly hydrophilic structure and the availability of abundant functional groups. Furthermore, the efficient selectivity originating from their tissue resembled nature makes them a more suitable and promising candidate for hydrogels having sensor features [3,12–15]. Although these hydrogels have the above-mentioned advantages, their non-conductive characteristic and insufficient mechanical performance should be improved for a more effective sensor process [16–19]. To gain electroconductive properties and enhance mechanical performance, either incorporation of conductive particles such as graphene and its derivatives into the polymeric network or the usage of conductive polymers (CPs) such as polypyrrole, poly(3,4-ethylenedioxythiophene) polystyrene sulfonate (PEDOT:PSS), polyaniline (PANI) in the hydrogel structure have been widely carried out as a facile route [20–24]. Among graphene family materials, reduced graphene oxide (rGO) has been commonly employed to possess mechanical strength due to its reinforcement effect and also electrical conductivity to hydrogels [25–27]. Besides, the highly hydrophilic and porous structure of rGO supplying the fast diffusion of target molecules and the ultimate bioconjugation arisen from the covalent/non-covalent bonding with

* Correspondence to: Marmara University, Department of Chemical Engineering, 34854 Istanbul, Turkey.
E-mail addresses: didem.aycan@marmara.edu.tr (D. Aycan), neslihan.alemdar@marmara.edu.tr (N. Alemdar).

https://doi.org/10.1016/j.mtcomm.2023.105745
Received 28 October 2022; Received in revised form 27 December 2022; Accepted 2 March 2023
Available online 5 March 2023

biomolecules could be enhanced the sensitivity and selectivity of the hydrogel based-sensors [28–30].

In the family of CPs, PANI is one of the most preferred polymeric materials in the production of ECHs because of its adjustable electrical conductivity, facile and easy synthesis route, unique redox properties, environmental stability, and better compatibility with biopolymers [31–34]. Introducing PANI into the hydrogel network not only allows the combination of the electrical conductivity capability of CPs and the distinctive characteristics of hydrogels but also enables good elasticity and mechanical strength to the hydrogel as the critical parameters for sensor applications [35,36].

In the light of these, we developed an effective approach to produce the HA-based ECH with improved mechanical properties by using rGO and PANI as a non-enzymatic glucose sensor in the current study. HA, which is a commonly-preferred polysaccharide in bio-based applications [37–40], was chosen as the main component of the hydrogel network in order to benefit from its high selectivity to various kinds of biomolecules including mono- (glucose, fructose, and galactose) and disaccharides (sucrose and lactose) owing to their similar nature [41–44]. HA is a crucial part of the extracellular matrix (ECM) and it has also an ability to mimic the natural tissues. Despite of these favorable features, a detailed literature survey revealed that there is surprisingly no study about the non-enzymatic glucose sensor based on HA. Although many researchers have reported various ECHs for the detection of glucose [45–47], there could not be encountered any study about HA-based non-enzymatic glucose sensor in the literature. Therefore, it can be stated that this study is the first report about the production of a non-enzymatic glucose sensor with a superior mechanical performance by using HA-rGO-PANI ternary formulation. In this new approach, while HA and rGO provided a porous hydrogel structure having a high surface area for the diffusion of biomolecules [29,48], both conductivity resources (PANI and rGO) would enable electron transfer across the path and improve mechanical properties owing to their superior features [49,50].

The hydrogel-based glucose sensor fabricated by using this new approach was characterized and evaluated in terms of mechanical performance and conductivity feature which are the key parameters for its usage in sensor applications. To demonstrate the utility of the produced HA-rGO-PANI hydrogel as a glucose sensor, its glucose sensitivity, selectivity, stability, reproducibility and storage measurements were carried out by using cyclic voltammetry (CV) and choronoamperometry (CA). The results showed that usage of both rGO and PANI in the polymeric network not only endowed considerable electrical conductivity to hydrogel (1.58×10^{-5} S/cm), but also significantly enhanced its compressive strength (992.1 kPa) and elastic modulus (23.4 kPa) compared to those of the bare HA hydrogel. It should be noted that these values approximately 500% and 1290% higher than that of the pure HA hydrogel, respectively. The currently developed HA-based sensor displayed high selectivity, stability and reproducibility, along with the high level of glucose sensitivity (as 421.42 $\mu A m M^{-1} cm^{-2}$), which is higher than a lot of reports related to the glucose sensing in the literature [51–57]. Based on all obtained results, it is worth to mention that this study could contribute to the usage of ECHs as sensors and could offer the guidance for creating composite networks with great mechanical performance in sensor applications.

2. Experimental

2.1. Materials

HA (food grade, Mw=8 $\times 10^5$ Da) was purchased from Heze Better Biochemical Co. (Shandong, China). D-(+)-glucose anhydrous (≥ 97.5%), ascorbic acid, uric acid (≥ 98%), D-sorbitol (≥ 98%), hydrochloric acid (HCl, 37%), potassium nitrate (KNO_3), ethanol (EtOH), methanol (MeOH), hydrogen peroxide (H_2O_2, 30%), potassium permanganate ($KMnO_4$), sulfuric acid (H_2SO_4, 98%), sodium hydroxide (NaOH), ammonium peroxodisulfate (APS) and aniline ($C_6H_5NH_2$) were obtained from Merck. Methacrylic anhydride (MA), photoinitiator (Irgacure 2959, 2-Hydroxy-4′-(2-hydroxyethoxy)− 2-methyl-propiophenone), phosphate buffer saline (PBS) tablet, graphite (powder < 20 μm, synthetic), hydrazine (35 wt% in H_2O) and 12–14 kDa cutoff dialysis tubing were purchased from Sigma Aldrich. All reagents were used as received without further purification.

2.2. Synthesis of rGO

Graphene oxide (GO) was synthesized from graphite according to modified Hummer's method [58–60]. Graphite powder (1 g) and KNO_3 (0.5 g) were slowly added to concentrated H_2SO_4 (23.3 ml) under ice-cooling and stirring. After cooling down, $KMnO_4$ (3 g) was gradually added to the solution. The mixture heated at 35 ºC in the sand bath and stirred for 30 min. Following that, the solution was diluted by adding distilled water (50 ml) and stirred at 90 ºC for 15 min. Then, water (167 ml) and H_2O_2 (5 ml, 30%) were added into the suspension, respectively. The resulting mixture was centrifuged and purified by multiple washing with HCl (10% v/v). The remaining slurry was dried at 65 ºC for 48 h to obtain solid GO. The GO suspension was prepared by dispersion of obtained GO in distilled water (200 ml). For reduction step, hydrazine (2 ml) was added into GO suspension under stirring at 100 ºC for 24 h. After cooling, the solution was purified by filtering and washing with methanol and distilled water, subsequently. Finally, the filtrate was dried at room temperature under vacuum for 3 days.

2.3. Synthesis of methacrylated HA (HA/MA)

HA-MA was synthesized by the reaction of HA with MA through an esterification reaction [61]. HA (1 g) was dissolved in distilled water under continuous stirring overnight. After complete dissolution, MA (4.8 ml) was added dropwise at 4 °C and the pH of the reaction medium was maintained at around 8 with 6 N NaOH in the dark for 24 h. Subsequently, produced HA/MA was precipitated in EtOH, filtered, washed and redissolved in distilled water, followed by dialysis against deionized water for 4 days. In the final step, the purified HA/MA was lyophilized and stored at 4 °C until further use.

2.4. Fabrication of HA/MA-rGO-PANI electroconductive hydrogels

HA/MA-rGO-PANI electroconductive hydrogels were produced following the procedure containing two different steps. In the first step, the prepolymer solution was prepared by mixing 1% (w/v) HA/MA dissolved in PBS with 3% (w/w) rGO suspension. After the addition of the photoinitiator ((2-Hydroxy-4′-(2-hydroxyethoxy)− 2-methyl-propiophenone), 0.5 w/v) into mixture, the final prepolymer solution was injected into round-glass molds and exposed to UV light (365 nm) for 30 min to allow the photocrosslinking. In the second step, the obtained hydrogels were immersed into 0.08 M ANI monomer solution and incubated for 12 h at room temperature. Equimolar amount of APS (0.08 M) was added into solution to initiate the polymerization of ANI and reaction was carried out for 3 h until dark-greenish color appeared, that confirms the formation of PANI. Then, hydrogels were immersed into distilled water for washing process and the produced HA-MA/rGO/PANI electroconductive hydrogels were dried overnight at room temperature.

2.5. Characterization

The oxidation of graphite and the reduction of GO were confirmed with Raman spectroscopy, which was recorded with a STEX-100 Compact Confocal Raman spectrometer at 532 nm excitation wavelength. The ratio of the intensity of D and G peaks (I_D/I_G) generally used to determine the quality of graphitization for carbon-based materials was also calculated. The structural characterization of synthesized rGO was investigated by using Hitachi High-Tech Transmission Electron

Microscope (TEM, HT7700) at an accelerating voltage of 105 kV. The samples for TEM analysis were prepared by dripping of rGO dispersed in ethanol on to the grids.

The produced HA/MA and HA/MA-rGO-PANI hydrogels were characterized by Fourier transform infrared spectroscopy (FT-IR). FT-IR spectroscopy was performed using a Perkin Elmer Spectrum One FT-IR with attenuated total (ATR) unit. The samples were scanned from 380 to 4000 cm^{-1}. The surface morphologies of the obtained hydrogels sputter coated with Au/Pd were investigated using scanning electron microscopy (SEM) (ZEISS EVO MA10).

2.6. Electrical conductivity

A Lucas Labs S-302 Four Point Resistivity Probe Equipment connected to a Gamry Instrument power source was used to characterize the electrical conductivity properties of the hydrogels originated from the sheet resistivity. The sheet resistance (ρ) is determined by supplying a constant current value between outer probes and measuring the voltage value between inner probes [58]. All hydrogel samples were tested in triplicate and the average values were recorded for each sample. ρ is calculated by using the following Eq. (1):

$$\rho = 2\pi sR \tag{1}$$

Where s is the probe spacing, R is the measured resistance value.

The conductivity value (σ) of the hydrogels was found by using the sheet resistivity data according to Eq. (2):

$$\sigma = \frac{1}{\rho} \tag{2}$$

2.7. Mechanical performance

Mechanical performance of the produced hydrogels were investigated using a Universal Testing Machine (Zwick Roell- Z1.0 Mechanical Test Machine equipped with a 50 N load cell) with 2 mm/min crosshead speed and 25 mm gauge length. All the hydrogel samples prepared as cylindrical shape were tested in triplicate. The stress-strain curves of the hydrogels were recorded at room temperature and the results were evaluated with regarding to elastic modulus (kPa) and compressive strength (kPa) for each sample. The elastic modulus values were extracted from the stress-strain curves of the hydrogels. The compressive strength (CS) values were calculated by using the Eq. (3):

$$CS = \frac{F_{max}}{A} \tag{3}$$

Where F_{max} corresponds to the maximum force (N), A represents the cross-sectional area of the sample (mm^2).

2.8. Electrochemical activity and sensor performance

The electrochemical measurements, which include the cyclic voltammetry (CV) and the choronoamperometry (CA), were performed by using a Potentiostat (GAMRY Instruments, Reference 600 Potentiostat/Galvanostat/ZRA) based on a three electrode cell configuration in PBS solution at 25 °C. While silver/silver chloride (Ag/AgCl) and platinum (Pt) wire were used as the reference and counter electrode respectively, the fabricated HA/MA-rGO-PANI electroconductive hydrogel was used as the working electrode for the CV and CA analyses.

All sensor measurements were carried out in PBS solution at room temperature under nitrogen atmosphere. Before sensing measurements, blank test was performed in glucose free PBS solution to observe redox activity of the electrode. 10 μL of glucose stock solution (in PBS) was gradually added into 5 ml of PBS and the response of the electrode to glucose derived from the interaction between them was investigated by CV analysis. The change of the peaks related to increasing glucose concentration was analyzed to determine the sensitivity and the selectivity of the electrode. Limit of detection (LOD) was calculated by using the Eq. (4):

$$LOD = \frac{3\sigma}{S} \tag{4}$$

Where σis the standard deviation obtained from calibration curve and S is the slope of the calibration curve.

Reproducibility of the sensor was examined by preparing 5 electrodes at the same time and testing sequentially each of them. The interference effect on the sensor response was tested using uric acid, ascorbic acid and sorbitol as interfering species. The responses of the sensor were observed by CA at an applied potential of 0.45 V. The long term cycling (100 cycles) was performed in CV analysis for stability test of the sensor.

2.9. Statistical analysis

GraphPad Prism Software (V.5, San Diego, USA) was used for statistical analysis. One way ANOVA was performed for a comparison test. The results were presented as means ± standard deviation (SD) within the 95% confidence level.

3. Results and discussions

3.1. Characterization of synthesized rGO

The structural changes of graphite, GO and rGO take place in the oxidation and reduction processes were examined through Raman analysis, which is a widely used a non-destructive technique to distinguish the disorder in the crystal structures of carbon-based materials [62]. The prominent peaks in the Raman spectra of carbonaceous materials are called as D and G bands. While D band is assigned to κ-point phonons of $A_{1\,g}$ symmetry, the G band represents the first-order scattering of $E_{2\,g}$ phonons [63]. As shown in Fig. 1A, the Raman spectrum of the graphite displays a D band peak at 1355 cm^{-1} and a G band peak at 1586 cm^{-1}. Besides, the 2D peak indicating overtone of the D peak appears at 2708 cm^{-1} in this spectrum. After oxidation, the G band broadened and shifted to 1597 cm^{-1} as a result of residual unmodified graphitic regions in GO structure [64]. The intensity ratio of the D band attributed to the degree of the disorder increased due to the decrease in the size of in-plane sp^2 domains by the oxidation process. The relative intensity ratio (I_D/I_G) used as an indication of the quality of graphitization increased from 0.27 to 0.79 after oxidation [65]. This increase could be explained by the disordered network resulted from the attachment of functional groups on the graphitic structure [66,67]. The I_D/I_G ratio increased to 1.10 after reduction. This increment suggests a decrease in the average size of sp^2 domains while an increase in the sp^2 cluster numbers, which reflects the formation of the more graphitic domain after reduction by removing most of the oxygenated functional groups from the structure [68,69]. ID/IG ratios were used to estimate the crystallite size of the synthesized GO and rGO according to the following Eq. (5) [70,71]:

$$L_a(nm) = \frac{2.4x10^{-10}\lambda^4}{I_{D/I_G}} \tag{5}$$

Where L_a is the crystallite size and λ is the wavelength of the laser source (532 nm).

While the crystallite size for GO was calculated as 24.3 nm, the crystallite size of rGO was found as 17.5 nm. This decrease, which was also in agreement with the increment of number of sp^2 domains in smaller size after reduction, could be attributed to the elimination of inter-layer attractive interactions and the decrement of the oxygen-containing functional groups in GO structure [72].

The structure of synthesized rGO was identified by TEM analysis. The

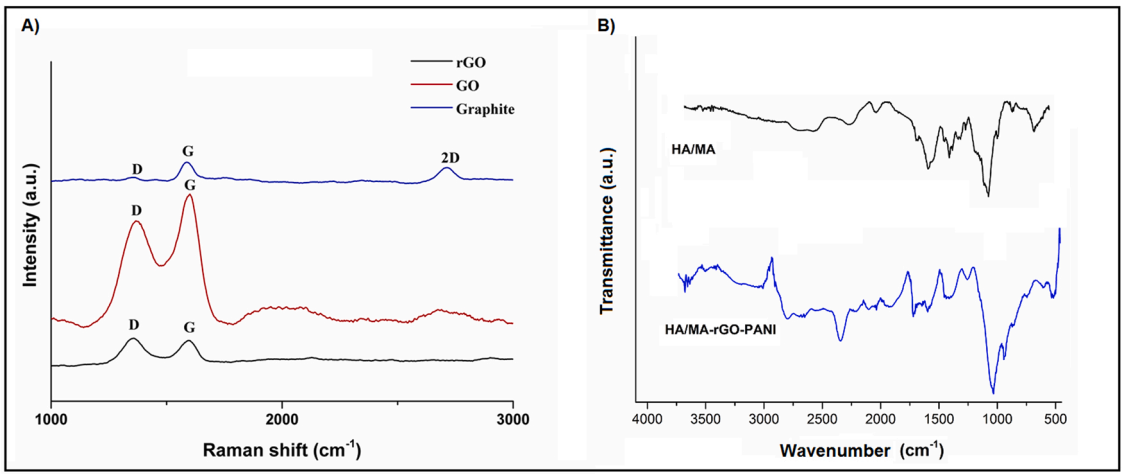

Fig. 1. RAMAN spectra (A) of graphite, GO and rGO and FT-IR spectra (B) of HA/MA and HA/MA-rGO-PANI hydrogels.

obtained TEM micrographs (Fig. 2) demonstrated the typical wrinkled pattern of the rGO structure that originated from the removal of hydroxyl and epoxide groups after the reduction process [73]. As a result of this, the repulsion between negatively charged groups in the structure decreased, which leads to the irregular veil-like layers [74]. The other important point observed from the TEM images was the highlight regions with the high contrast spots, which indicates the remaining functional groups in the rGO structure.

3.2. Fabrication and characterization of HA/MA-rGO-PANI conductive hydrogels

HA/MA-based ECHs were synthesized through the photocrosslinking mechanism that was demonstrated in Scheme 1.

For the structural characterization, HA/MA and HA/MA-rGO-PANI hydrogels were compared each other by using FT-IR analysis. As shown in Fig. 1B, the FT-IR spectra of HA/MA exhibited the characteristic peaks at 1716 cm^{-1} and 1449 cm^{-1} corresponding C═O (carbonyl) stretching and C═C (carbon-carbon double bonds) of conjugated system, respectively [75]. The presence of these bands confirmed successfully insertion of methacrylate groups into the HA backbone. In the

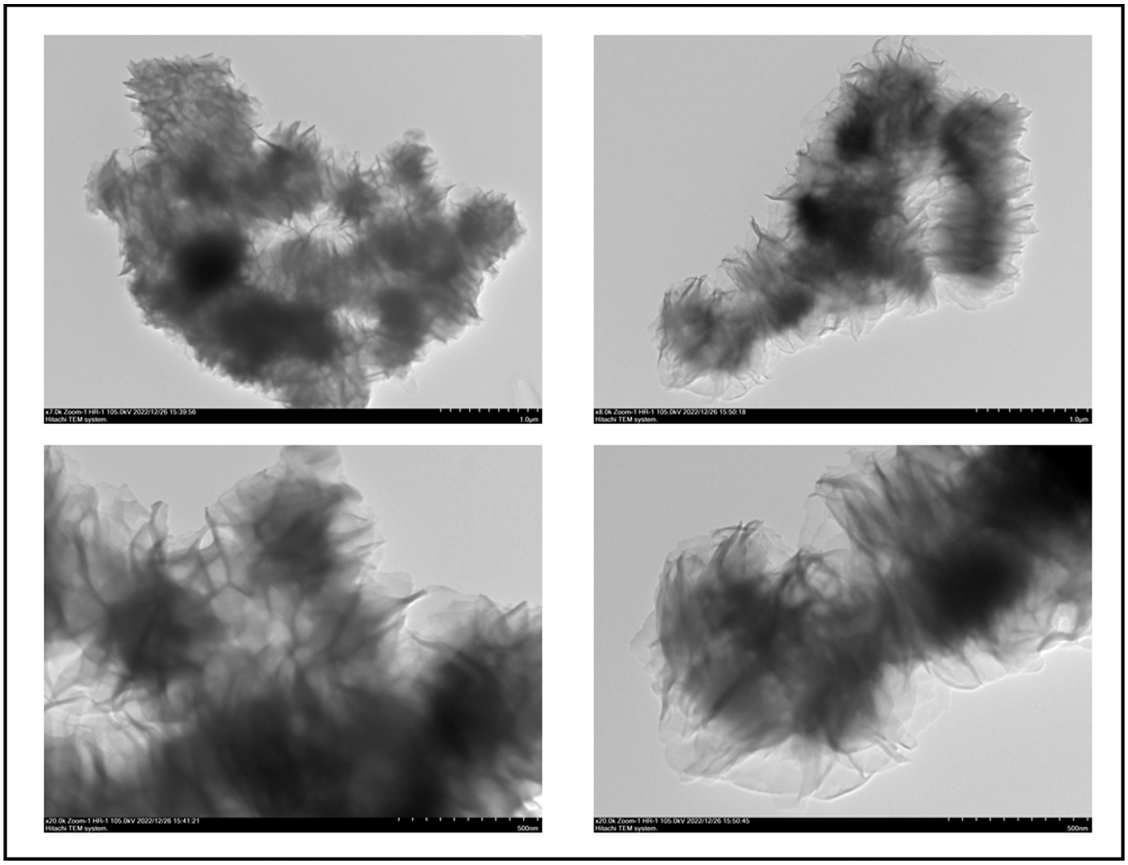

Fig. 2. TEM micrographs of synthesized rGO at different magnifications.

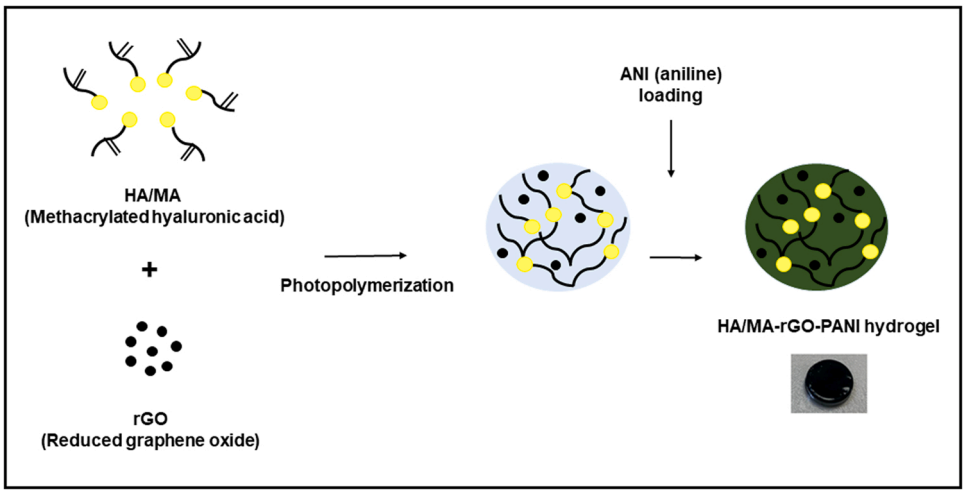

Scheme 1. Schematic representation of production of HA/MA-rGO-PANI hydrogel.

spectrum of HA/MA-rGO-PANI hydrogel, decreasing of the peaks for the bands at about 1070, 1400 and 1700 cm^{-1} compared to pure HA/MA hydrogel indicated the hydrogen bonding between oxygen containing groups of rGO and C═O (carbonyl) groups of HA/MA [76]. The main characteristic peaks for PANI were also observed at 1558, 1487 and 1238 cm^{-1}, which correspond to stretching vibrations of quinone ring, benzenoid ring and C-N stretching vibration of secondary amine, respectively as well as the characteristic peaks of HA/MA structure [77–79]. Additionally, slight shifting of the peaks of HA/MA-rGO-PANI hydrogel compared to HA/MA hydrogel indicated the $\pi - \pi$ interactions between rGO and PANI structure [80].

SEM analysis was performed to investigate the morphology of HA/MA and HA/MA-rGO-PANI hydrogels, as presented in Fig. 3. The SEM image of HA/MA hydrogel (Fig. 3A) exhibited 3D network structure, which is a characteristic morphology for a hydrogel. In the SEM image of HA/MA-rGO-PANI hydrogel (Fig. 3B, C), an interconnected network-like structure was observed by the introduction of both rGO and PANI to the HA/MA hydrogel. As more clearly seen in the SEM images of HA/MA-rGO-PANI hydrogel, while rGO was appeared as the layered structure with distinct edges entrapped in the PANI matrix, PANI showed densely stacked morphology with sphere-like form in the hydrogel network owing to the self-assembling characteristic of PANI [81]. The

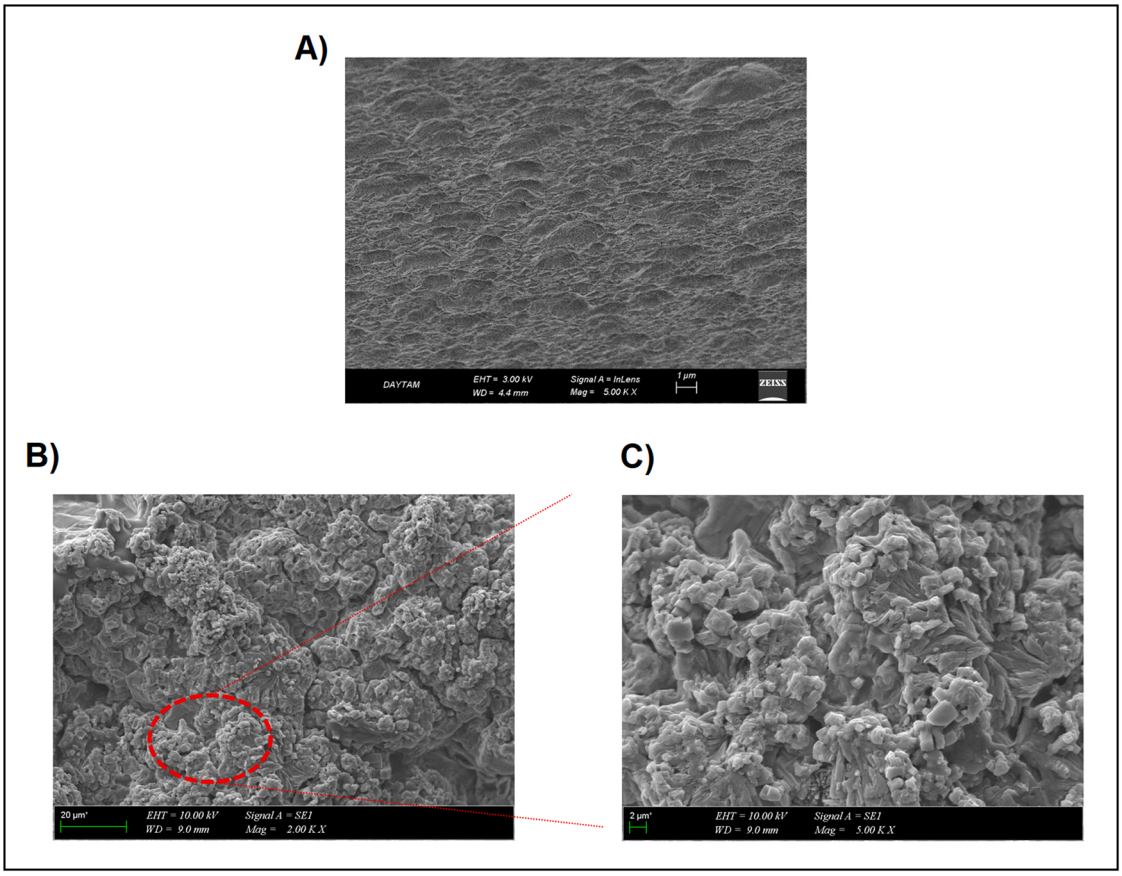

Fig. 3. SEM images of HA/MA hydrogel (A) and HA/MA-rGO-PANI (B, C) hydrogel at different magnifications.

voids in the network created by the incorporation of rGO into structure were partially filled with PANI spheres that could be explained by the dispersion forces originated from the hydrophobic nature of PANI molecules [82]. Additionally, this morphology might be offered a continuous physical pathway for more sufficient transfer and separation of electrons [80].

3.3. Electrical conductivity

ECHs employed as a biomaterial should be possessed an adequate level of electrical conductivity to promote their performance and productivity in sensor applications [83]. Based on this, to evaluate the fabricated hydrogel in terms of electrical conductivity, the sheet resistance of HA/MA-rGO-PANI hydrogel was measured via a four-point probe method. Hydrogel sample was tested three times. Table 1 shows all conductivity results which were calculated by using the sheet resistance values. These results were also presented as a graph (Fig. 4). HA/MA-rGO-PANI hydrogel exhibited sufficient electrical conductivity as 1.58×10^{-5} S/cm, which is in the range of conductivity for desired application field [84]. There are four important contributions provided by rGO and PANI to electrical conductivity in the hydrogel network structure, i) the sp2-hybridized carbon system restored by the reduction process of GO contributed to the electrical conductivity of the produced hydrogel, ii) the well-distributed rGO particles in the hydrogel network form the effective and conductive pathway leading in an electroconductive structure [85], iii) the polyconjugated planar structure of PANI offers an electron transport path owing to phenyl rings and intertwined PANI chains within the network, iv) the electron delocalization of polaron/bipolaron structures of PANI also provides improved electrical conductivity to the hydrogel [86,87]. When the results are examined, it is clear that the usage of both rGO and PANI in the network ensures adequate level of electrical conductivity to the hydrogel due to the synergistic effect of them.

3.4. Mechanical performance

Mechanical performance is one of the key parameter to develop ECHs employed as a biosensing material. Since insufficient mechanical properties of the hydrogels have still remained a challenge for their practical usage in desired application field, fabrication of ECHs with enhanced mechanical strength is being an attractive approach to meet the special requirements of sensor applications. Therefore, the compressive test (Fig. 5A) was conducted to evaluate mechanical performance of the produced HA/MA and HA/MA-rGO-PANI hydrogels with regards to compressive strength and elastic modulus. The compressive strength of HA/MA and HA/MA-rGO-PANI hydrogels (Fig. 5B) were calculated as 191.8 and 992.1 kPa, respectively. This significant improvement could be explained by the development of mechanically stronger structures due to the reinforcement effect of rGO particles and rigid PANI chain [26,27,88,89]. While the strong physical interactions including hydrogen bonding and Van der Waals force between rGO and polymeric network lead to increase the mechanical strength of the HA-based hydrogel, the electrostatic interactions between PANI and the polymeric network as well as the rigid nature of the PANI also supported to strengthen the hydrogel structure [90].

Table 1
Conductivity values of hydrogel samples.

Sample	Resistance (Ω)	Sheet resistivity (Ω. cm)	Conductivity (S/cm)	Average Conductivity (S/cm)
HA/MA	NA	NA	NA	NA
HA/MA-rGO-PANI	7.7×10^4 8.1×10^4 8.2×10^4	0.61×10^5 0.64×10^5 0.65×10^5	1.64×10^{-5} 1.56×10^{-5} 1.54×10^{-5}	1.58×10^{-5}

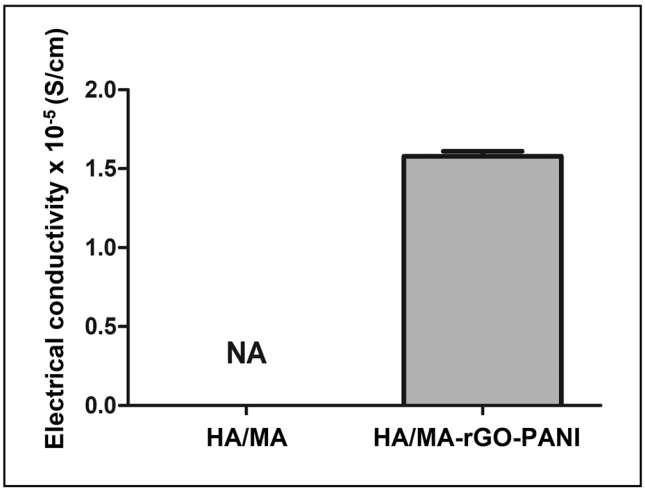

Fig. 4. Electrical conductivity of the HA/MA and HA/MA-rGO-PANI hydrogels.

Furthermore, introduction of rGO enabled to the more uniformed distribution of stress transfer at the polymer matrix resulted in a mechanically stronger structure. As shown in Fig. 5C, elastic modulus of the hydrogels increased substantially with the incorporation of rGO and PANI into hydrogel structure. The elastic modulus of HA/MA-rGO-PANI hydrogel reached the maximum value as 23.4 kPa which was approximately 20 times higher than HA/MA hydrogel that provided favorable flexibility and elasticity to hydrogels as a result of the decrement effect of PANI on the brittle and fragile structure of hydrogels. These results demonstrated that the superior mechanical performance, namely good elasticity and mechanical strength was ensured by the fabrication of interpenetrating network containing both PANI and rGO in its structure and the obtained HA/MA-rGO-PANI hydrogel with enhanced mechanical properties have a great potential to employ as a sensing material in further studies.

3.5. Electrochemical activity and sensor performance of HA-based hydrogel

The electrochemical behavior of produced HA-based hydrogel sensor was determined in the absence and presence of glucose through CV measurement, whose curves were monitored in the voltage range between − 0.8 V and 0.8 V at a scan rate of 100 mV/s in PBS. As presented in Fig. 6A, although there is no addition of glucose to the electrolyte at the beginning of the sensitivity measurement, HA/MA-rGO-PANI hydrogel sensor showed a pair of reduction and oxidation peak current due to the common behavior of PANI-containing networks in neutral pH medium [49,91]. Upon addition of glucose, the presence of redox peaks and the noticeable increase in the peak current values approved the electroactive behavior of the developed HA/MA-rGO-PANI hydrogel sensor towards glucose.

The plausible glucose detection mechanism based on the chemisorption of the glucose on the surface of HA/MA-rGO-PANI hydrogel electrode was depicted in Scheme 2. The observed redox current in CV measurement originated from the transformation from emeraldine state to leucoemeraldine state of PANI structure, which enables the formation of an ion-dipole between glucose molecules and $–HN^+$ group of PANI [92,93]. After the addition of glucose solution in PBS, leucoemeraldine state was converted into the emeraldine state by accepting an electron and this behavior created an electron transport system supplying the electron transfer from glucose to the HA/MA-rGO-PANI hydrogel electrode [94]. It is also worth emphasizing that PBS medium used in sensing measurements has two significant contributions, i) it provided to detect glucose at physiological conditions, ii) it supplied hydroxyl ions, which received the electrons from the surface of the HA/MA-rGO-PANI

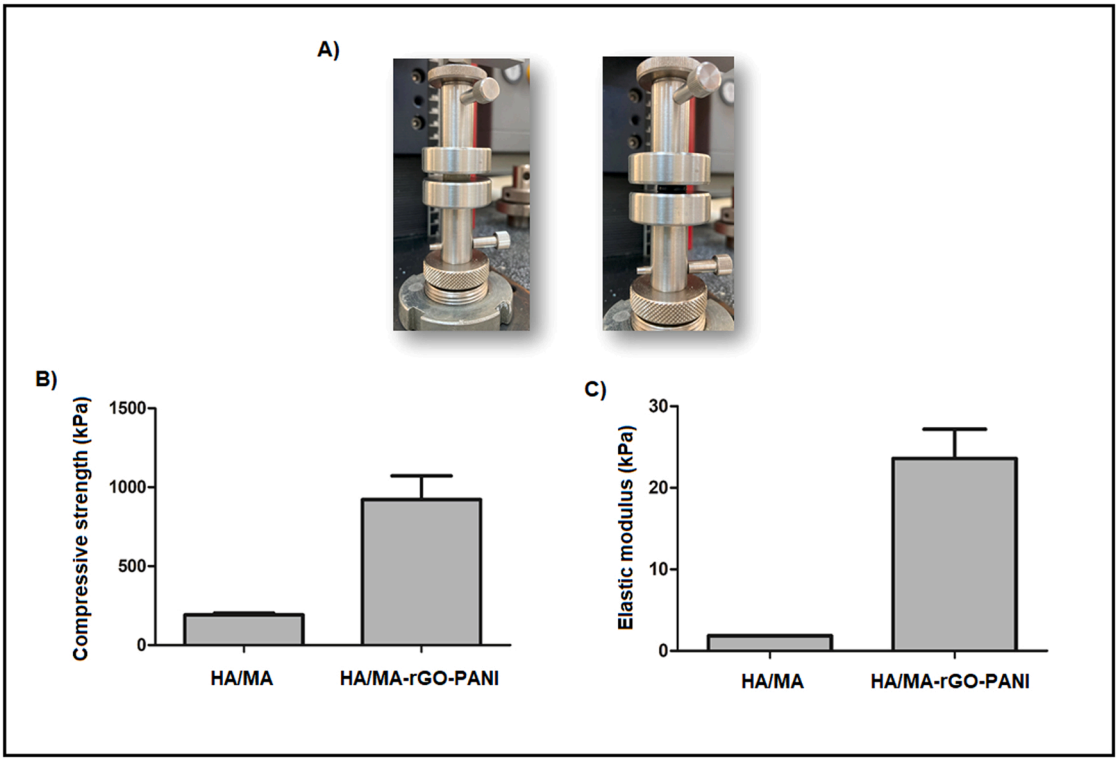

Fig. 5. Images of HA/MA and HA/MA-rGO-PANI hydrogels during compressive test (A), compressive strength (B) and elastic modulus (C) of produced HA/MA and HA/MA-rGO-PANI hydrogels.

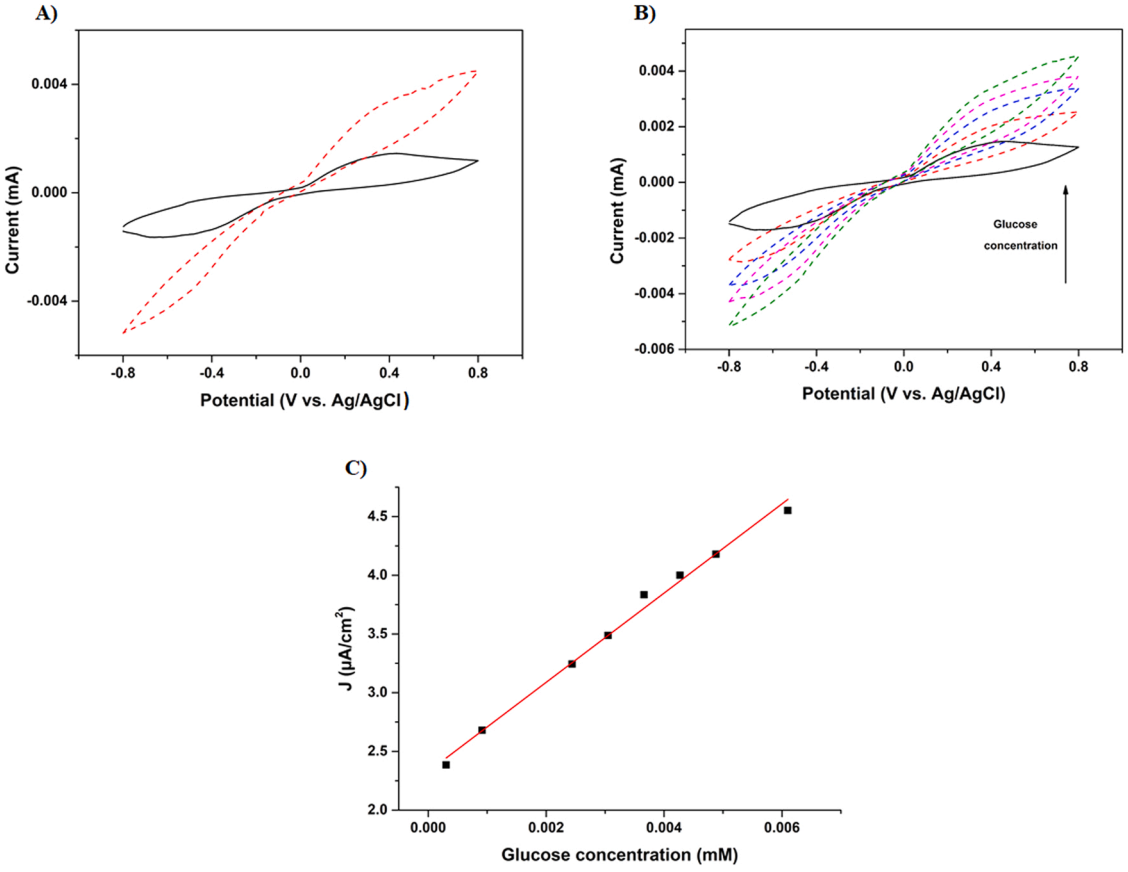

Fig. 6. Cyclic voltammetric responses of HA-based hydrogel sensor in the presence and absence of glucose in PBS (A), Cyclic voltammetric responses of HA/MA-rGO-PANI hydrogel sensor to increasing glucose concentration in PBS (B) and the calibration curve of current density vs. glucose concentration (C).

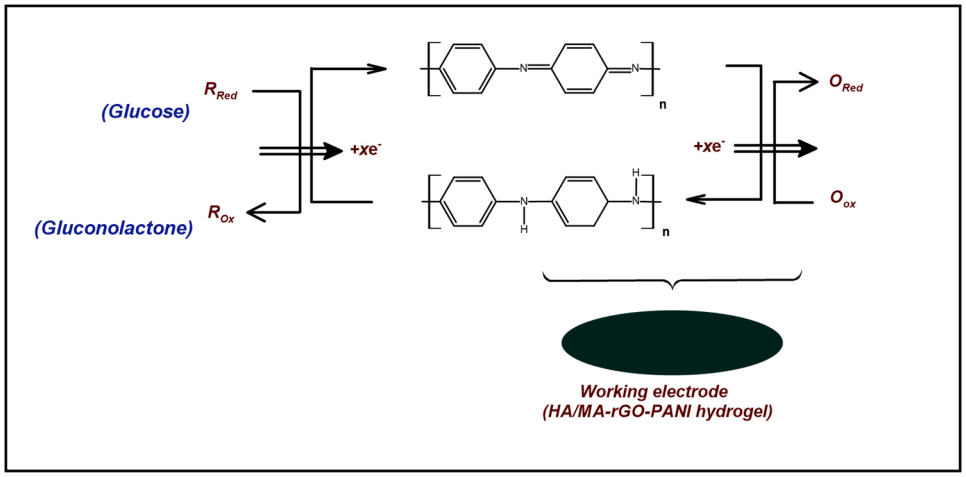

Scheme 2. The schematic representation of the plausible non-enzymatic glucose sensing mechanism of the produced HA/MA-rGO-PANI hydrogel electrode.

hydrogel electrode. And thus, the highly reactive oxygenated sites were generated which leads to the oxidation of the glucose molecules to the gluconolactone [95]. Furthermore, the produced HA/MA-rGO-PANI hydrogel electrode could adsorb more glucose molecules owing to the 3D structure of hydrogel containing both rGO and PANI, the integration of which might enhance the electrocatalytic activity of the sensing material.

The glucose sensing characteristic of the sensor was also evaluated by increasing glucose concentration (Fig. 6B). It is clearly seen that the redox peaks current gradually increased with the increment of glucose concentration, attributing electro-oxidation/reduction of glucose and sufficient electrical conductivity of the produced network. The calibration curve (Fig. 6C) exhibited a linear response with the correlation coefficient of 0.993 based on the glucose concentration. The glucose sensitivity was determined from the linear range of the calibration curve (0.3–6 μM) by using the following Eq. (6):

$$Sensitivity\left(\mu AmM^{-1}cm^{-2}\right) = \frac{\Delta current(\mu A)}{\Delta glucoseconcentration(mM)xelectrodearea(cm^2)} \quad (6)$$

The sensitivity value and the detection limit were found as 379.92 μA/mMcm^2 and 0.3 μM, respectively.

The chronoamperometric characterization of HA/MA-rGO-PANI hydrogel sensor was also carried out with the consecutive injection of glucose solution (from 0.3 μM to 5 μM) into PBS medium at a constant potential of 0.45 V. The obtained sensor's current-time response to increasing glucose concentration at every 30 s was measured and the results were plotted as shown in Fig. 7. A linear increase in the current response within 2–3 s by the increasing glucose concentration demonstrated the fast glucose sensing ability of the HA/MA-rGO-PANI hydrogel sensor. The calibration plot of the glucose concentration vs. determined current density values presented a wide linear range with the linear regression coefficient (R) of 0.996. The sensitivity value was calculated from the linear range of the obtained calibration curve as 421.42 μA/mMcm^2 in the amperometric measurement. The obtained higher (about 10%) sensitivity value comparing with the sensitivity (379.92 μA/mMcm^2) found in the CV measurement could be attributed to the improved mass transfer under the static operation conditions.

As listed in Table 2, the performance of non-enzymatic HA-based hydrogel sensor is superior from the other reported studies in the literature. In particular, obtained sensitivity is one of the highest value ever determined for the non-enzymatic glucose sensors. These remarkable results could be related to the following aspects: (i) ECM-like nature of HA supports to easily capture of glucose, (ii) interconnected porous 3D structure obtained by the incorporation of rGO into polymeric network

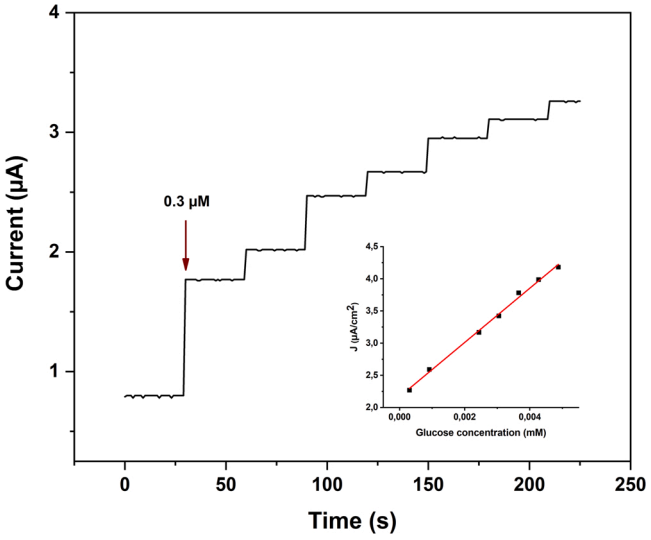

Fig. 7. Amperometric responses of HA/MA-rGO-PANI hydrogel sensor to increasing glucose concentration in PBS at 0.45 V integrated with the calibration curve of the current density vs. glucose concentration.

Table 2
Comparison of the analytical performance of non-enzymatic glucose sensors.

Working electrode	Sensitivity ($\mu AmM^{-1}cm^{-2}$)	LOD (μM)	Reference
Pdnanowire-PANI	146.6	0.7	[53]
pPDA(p-phenylene diamine)-GO	24.81	NR	[52]
Pt-GO	137.4	NR	[56]
Pd-Ni-rGO	37.5	0.15	[55]
Pd-Mn-rGO	52.16	1.25	[57]
CTS-CST(cadmium stannate)-PANI	$1.32x10^{-3}$	0.5	[51]
PANI-CNT (carbon nanotubes)	10.89	1.3	[54]
HA/MA-rGO-PANI	**421.42**	**0.3**	**Current study**

offers open channels for the permeability of glucose molecules, and (iii) the combination of rGO and PANI as the conductivity sources promotes the electron transfer rate [37,96,97].

The stability, reproducibility and storage tests were performed to examine the usage of HA-based hydrogel in practical sensor

applications. The stability of the HA-MA/rGO/PANI hydrogel sensor was evaluated by running CV measurement for 100 consecutive cycles at 100 mV/s containing 100 μL glucose solution in PBS. As demonstrated in Fig. 8A, there was no significant change of the current response of the sensor after long-term cycling, indicating that fabricated HA-MA/rGO/PANI hydrogel sensor has excellent stability. Additionally, the storage stability of the produced HA-MA/rGO/PANI hydrogel biosensor was observed over a 30-day period. The prepared sensor was kept in PBS solution at room temperature. The sensitivity values were calculated once a week to determine relative sensitivity (Fig. 8B) for the fabricated sensor. Obtained results revealed that the sensitivity value of the sensor remained nearly 93.6% of its initial sensitivity value even after 30 days, which could be also attributed to the synergistic effect of the rGO and PANI on the mechanical performance of the hydrogel network. It is worth to emphasize that obtained storage stability is better than the many previous studies about the glucose sensing in the literature. For example, Li et al. reported that PdNW (nanowire)-PANI network retained 93.4% of its stability after just 7 days and another study presented 5.6% of stability loss over only 2 weeks period that were relatively low storage performances comparing that of our study [53,56].

For the reproducibility test, five identical HA-MA/rGO/PANI hydrogel biosensor were prepared. Following that, they were tested by adding a series of concentrations of glucose. The sensitivity values of each hydrogel sensor were calculated and demonstrated in Fig. 9. The relative standard deviation (RSD) was found as 4.8% (n = 5), confirming adequate reproducibility in the formation of HA-based hydrogel sensor.

The non-enzymatic glucose detection could be disturbed by several interfering species such as uric acid, ascorbic acid and sorbitol, which are normally present with glucose in human blood. Despite the concentration of these electroactive compounds is lower compared to glucose concentration in blood sample, they could also generate an electrochemical signal because of the structural resemblance and common ion effect. Thus, the anti-interference test (Fig. 10A) was carried out with the successive addition of 4.0 mM of glucose and 0.1 mM of uric acid, ascorbic acid and sorbitol in order to observe the effect of these interfering reagents. As shown in Fig. 10B, the interfering species induced negligible responses (about 2.5–5% of that produced by glucose) in the amperometric test. These observations confirmed that developed HA/MA-rGO-PANI hydrogel sensor have good selectivity and excellent anti-interference performance for glucose detection owing to the recognition ability of HA for biomolecules as well as its favorable interactions with target analytes [41,47].

Based on the all results, it was concluded that HA-based hydrogel could be utilized as a promising non-enzymatic sensor with excellent

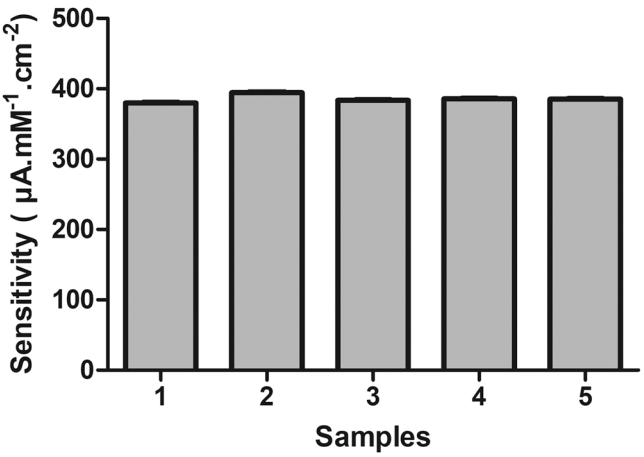

Fig. 9. Sensitivity values of the identical HA-MA/rGO/PANI hydrogel sensors.

selectivity, sensitivity, low detection limit and long-term stability and storage performance for glucose detection in future studies.

4. Conclusion

ECHs have received a great deal of attention for sensor applications since they integrate remarkable features of the hydrogel network and the electrochemical properties of conductive materials. In this study, HA-based ECH was successfully produced by photocrosslinking mechanism by the incorporation of rGO and then loading of PANI as conducting materials into the polymeric network. While numerous studies have reported to fabricate ECHs employed as biosensing materials in the literature, HA-based ECH consisting of the HA-rGO-PANI ternary combination was used as a non-enzymatic glucose sensor for the first time in the current study. Introducing rGO and PANI into hydrogel structure not only endowed efficient electrical conductivity to hydrogel but also provided improved mechanical performance in terms of compressive strength and elastic modulus, which are critical requirements for sensor applications. The developed HA-based hydrogel sensor exhibited good electrochemical activity to glucose molecules with a low detection limit (0.3 μM), high sensitivity (421.42 $\mu AmM^{-1}cm^{-2}$) and selectivity in the presence of various interfering species such as uric acid, ascorbic acid and sorbitol and also excellent long-term stability. It should be clearly pointed out that these promising sensor performances of the novel HA/MA-rGO-PANI hydrogel are superior to those of great numbers of sensor materials previously reported and employed for non-enzymatic glucose

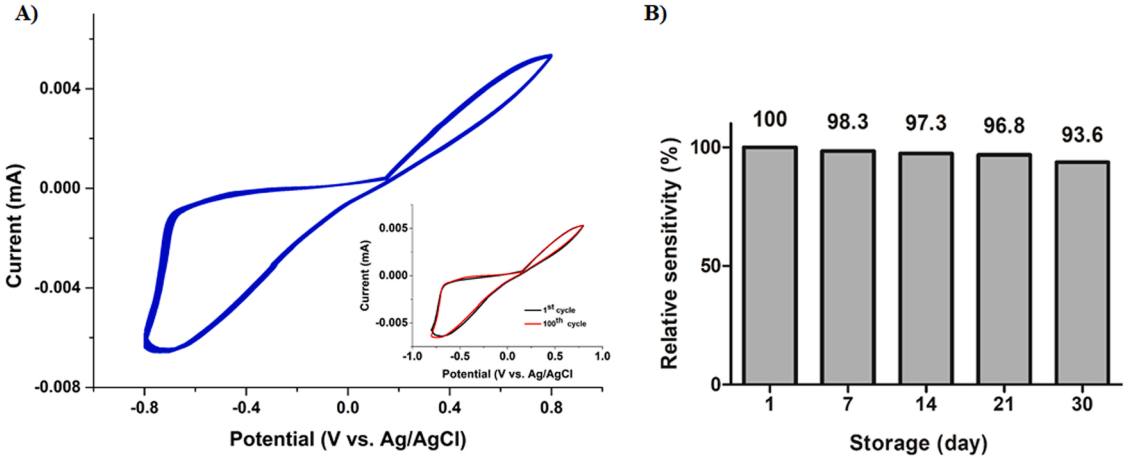

Fig. 8. The long-term stability test of HA-MA/rGO/PANI hydrogel sensor over 100 cycles (A) and the storage stability of HA-MA/rGO/PANI hydrogel sensor for 30 days (B).

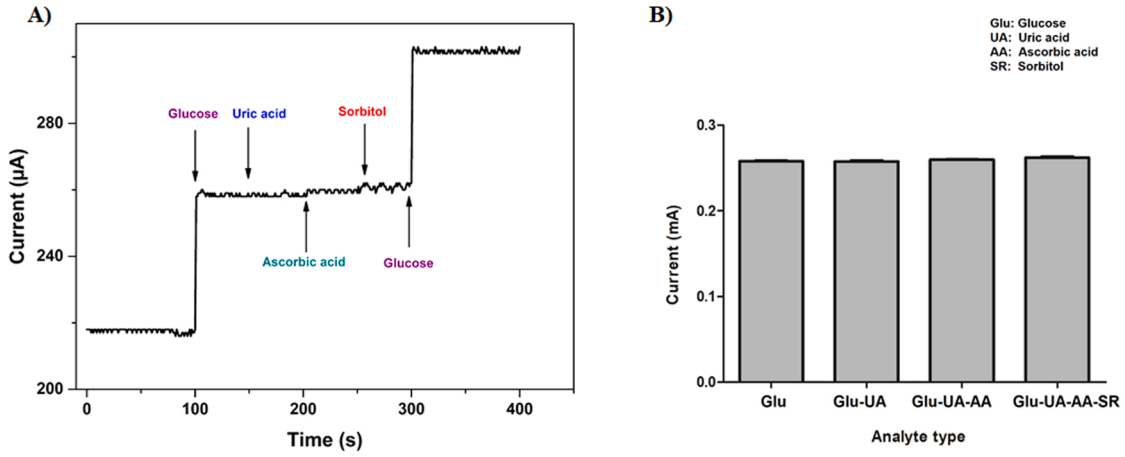

Fig. 10. Amperometric response of HA-MA/rGO/PANI hydrogel sensor after the successive addition of glucose, uric acid, ascorbic acid and sorbitol in PBS at 0.45 V (A) and the selectivity study involving glucose with different interfering reagents (B).

detection in the literature. All acquired results showed that HA/MA-rGO-PANI hydrogel would be an attractive candidate for further sensitive non-enzymatic glucose detection applications. Furthermore, this study offers broad-visioned and new opportunities for HA-based hydrogels systems in the sensor field.

CRediT authorship contribution statement

Didem Aycan: Methodology, Investigation, Visualization, Validation, Data curation, Writing – original draft, Writing – review & editing. **Fatma Karaca:** Resources, Project administration, Funding acquisition, Visualization. **Neslihan Alemdar:** Supervision, Conceptualization, Resources, Project administration, Methodology, Visualization, Validation, Data curation, Writing – original draft, Writing – review & editing.

Declaration of Competing Interest

The authors declare that they have no known competing financial interests or personal relationships that could have appeared to influence the work reported in this paper.

Data Availability

Data will be made available on request.

Acknowledgements

The financial support for this study was granted by the Scientific Research Projects Commissions (BAPKO) of Marmara University (Project no: FEN-C-DRP-130319-0073).

References

[1] F. Pinelli, L. Magagnin, F. Rossi, Progress in hydrogels for sensing applications: a review, Mater. Today Chem. 17 (2020), 100317.
[2] X. Sun, S. Agate, K.S. Salem, L. Lucia, L. Pal, Hydrogel-based sensor networks: compositions, properties, and applications—a review, ACS Appl. Bio Mater. 4 (2020) 140–162.
[3] C. Cui, Q. Fu, L. Meng, S. Hao, R. Dai, J. Yang, Recent progress in natural biopolymers conductive hydrogels for flexible wearable sensors and energy devices: materials, structures, and performance, ACS Appl. Bio Mater. 4 (2020) 85–121.
[4] X. Guo, W. Huang, J. Tong, L. Chen, X. Shi, One-step programmable electrofabrication of chitosan asymmetric hydrogels with 3D shape deformation, Carbohydr. Polym. 277 (2022), 118888.
[5] J. Körner, C.F. Reiche, H.-Y. Leu, N. Farhoudi, J. Magda, F. Solzbacher, A sensor platform for smart hydrogels in biomedical applications, Multidiscip. Digit. Publ. Inst. Proc. 2 (2018) 1006.
[6] G.C. Le Goff, R.L. Srinivas, W.A. Hill, P.S. Doyle, Hydrogel microparticles for biosensing, Eur. Polym. J. 72 (2015) 386–412.
[7] D. Zhang, J. Jian, Y. Xie, S. Gao, Z. Ling, C. Lai, et al., Mimicking skin cellulose hydrogels for sensor applications, Chem. Eng. J. 427 (2022), 130921.
[8] Z.S. Nishat, T. Hossain, M.N. Islam, H.P. Phan, M.A. Wahab, M.A. Moni, et al., Hydrogel Nanoarchitectonics: An Evolving Paradigm for Ultrasensitive Biosensing, Small, (2022) 2107571.
[9] K.S. Salem, V. Naithani, H. Jameel, L. Lucia, L. Pal, Lignocellulosic fibers from renewable resources using green chemistry for a circular economy, Glob. Chall. 5 (2021), 2000065.
[10] A. Sinha, P.K. Kalambate, S.M. Mugo, P. Kamau, J. Chen, R. Jain, Polymer hydrogel interfaces in electrochemical sensing strategies: a review, TrAC, Trends Anal. Chem. 118 (2019) 488–501.
[11] J. Tavakoli, Y. Tang, Hydrogel based sensors for biomedical applications: an updated review, Polymers 9 (2017) 364.
[12] M. Jian, Y. Zhang, Z. Liu, Natural biopolymers for flexible sensing and energy devices, Chin. J. Polym. Sci. 38 (2020) 459–490.
[13] W. Lipińska, K. Siuzdak, J. Karczewski, A. Dołęga, K. Grochowska, Electrochemical glucose sensor based on the glucose oxidase entrapped in chitosan immobilized onto laser-processed Au-Ti electrode, Sens. Actuators B: Chem. 330 (2021), 129409.
[14] Z. Zhang, Y. Xu, Y. Zhang, B. Ma, Z. Ma, H. Han, Antifouling and sensitive biosensor based on multifunctional peptide and urease@ ZIFs for metal matrix protease-7, Sens. Actuators B: Chem. 364 (2022), 131844.
[15] R.M. O'Dea, J.A. Willie, T.H. Epps III, 100th anniversary of macromolecular science viewpoint: polymers from lignocellulosic biomass. Current challenges and future opportunities, ACS Macro Lett. 9 (2020) 476–493.
[16] Y. Chen, W. Wu, J. Yu, Y. Wang, J. Zhu, Z. Hu, Mechanical strong stretchable conductive multi-stimuli-responsive nanocomposite double network hydrogel as biosensor and actuator, J. Biomater. Sci., Polym. Ed. 31 (2020) 1770–1792.
[17] S. Himori, T. Sakata, Free-standing conductive hydrogel electrode for potentiometric glucose sensing, RSC Adv. 12 (2022) 5369–5373.
[18] R. Wang, N. Li, L. Zhang, L. Gao, W. Hong, T. Jiao, Facile construction of gelatin/polyacrylamide acrylic acid/sodium alginate-based triple-network composite hydrogels with excellent mechanical performances, Integr. Ferroelectr. 227 (2022) 98–109.
[19] E. Zhang, J. Yang, W. Liu, Cellulose-based hydrogels with controllable electrical and mechanical properties, Z. Phys. Chem. 232 (2018) 1707–1716.
[20] K. Abu-Rabeah, R.S. Marks, Impedance study of the hybrid molecule alginate–pyrrole: demonstration as host matrix for the construction of a highly sensitive amperometric glucose biosensor, Sens. Actuators B: Chem. 136 (2009) 516–522.
[21] H. Al-Sagur, E. Kaya, M. Durmuş, T. Basova, A. Hassan, Amperometric glucose biosensing performance of a novel graphene nanoplatelets-iron phthalocyanine incorporated conducting hydrogel, Biosens. Bioelectron. 139 (2019), 111323.
[22] R.D. Pyarasani, T. Jayaramudu, A. John, Polyaniline-based conducting hydrogels, J. Mater. Sci. 54 (2019) 974–996.
[23] N. Singh, M.A. Ali, P. Rai, I. Ghori, A. Sharma, B. Malhotra, et al., Dual-modality microfluidic biosensor based on nanoengineered mesoporous graphene hydrogels, Lab a Chip 20 (2020) 760–777.
[24] Y. Wei, Q. Zeng, M. Wang, J. Huang, X. Guo, L. Wang, Near-infrared light-responsive electrochemical protein imprinting biosensor based on a shape memory conducting hydrogel, Biosens. Bioelectron. 131 (2019) 156–162.
[25] S. Xia, S. Feng, Z. Deng, Q. Liang, X. Xiang, H. Xie, The role of reduced graphene oxide as a "2D flexible crosslinking point" in composite hydrogels, Polym. Eng. Sci. 62 (2022) 416–425.
[26] X. Xiang, Q. He, S. Xia, Z. Deng, H. Zhang, H. Li, Study of capacitance type flexible electronic devices based on polyacrylamide and reduced graphene oxide composite hydrogel, Eur. Polym. J. 171 (2022), 111200.

[27] L. Zhang, Q. Jiang, Y. Zhao, J. Yuan, X. Zha, H. Xie, et al., Strong and tough PAm/SA hydrogel with highly strain sensitivity, J. Renew. Mater. 10 (2022) 415.
[28] E.J.C. Amieva, J. López-Barroso, A.L. Martínez-Hernández, C. Velasco-Santos, Graphene-based materials functionalization with natural polymeric biomolecules, Recent Adv. Graph. Res. 1 (2016) 257–298.
[29] S. Shahriari, M. Sastry, S. Panjikar, R.S. Raman, Graphene and graphene oxide as a support for biomolecules in the development of biosensors, nanotechnology, Sci. Appl. 14 (2021) 197.
[30] M. Thangamuthu, K.Y. Hsieh, P.V. Kumar, G.-Y. Chen, Graphene-and graphene oxide-based nanocomposite platforms for electrochemical biosensing applications, Int. J. Mol. Sci. 20 (2019) 2975.
[31] S.P. Ansari, A. Anis, Conducting polymer hydrogels, Polymeric Gels, Elsevier, 2018, pp. 467–486.
[32] L. Cao, S. Huang, F. Lai, Z. Fang, J. Cui, X. Du, et al., Sucrose in situ physically cross-linked of polyaniline and polyvinyl alcohol to prepare three-dimensional nanocomposite hydrogel with flexibility and high capacitance, Ionics 27 (2021) 3431–3441.
[33] J. Du, W. Zhu, Q. Yang, X. She, H. Wu, C. Tsou, et al., Strong conductive hybrid hydrogel electrode based on inorganic hybrid crosslinking, Colloid Polym. Sci. 300 (2022) 111–124.
[34] W. Zhang, P. Feng, J. Chen, Z. Sun, B. Zhao, Electrically conductive hydrogels for flexible energy storage systems, Prog. Polym. Sci. 88 (2019) 220–240.
[35] Y. Jiao, Y. Lu, K. Lu, Y. Yue, X. Xu, H. Xiao, et al., Highly stretchable and self-healing cellulose nanofiber-mediated conductive hydrogel towards strain sensing application, J. Colloid Interface Sci. 597 (2021) 171–181.
[36] T. Zhan, H. Xie, J. Mao, S. Wang, Y. Hu, Z. Guo, Conductive PNIPAM/CMCS/MWCNT/PANI hydrogel with temperature, pressure and pH sensitivity, ChemistrySelect 6 (2021) 4229–4237.
[37] M. Dovedytis, Z.J. Liu, S. Bartlett, Hyaluronic acid and its biomedical applications: a review, Eng. Regen. 1 (2020) 102–113.
[38] H. Mao, S. Zhao, Y. He, M. Feng, L. Wu, Y. He, et al., Multifunctional polysaccharide hydrogels for skin wound healing prepared by photoinitiator-free crosslinking, Carbohydr. Polym. 285 (2022), 119254.
[39] J. Xu, Y.L. Tsai, S.H. Hsu, Design strategies of conductive hydrogel for biomedical applications, Molecules 25 (2020).
[40] Y. Yang, L. Xu, J. Wang, Q. Meng, S. Zhong, Y. Gao, et al., Recent advances in polysaccharide-based self-healing hydrogels for biomedical applications, Carbohydr. Polym. 283 (2022), 119161.
[41] S. Park, Y.J. Kim, S. Park, H. Hong, J. Lee, S.I. Kim, et al., Rapid extraction and detection of biomolecules via a microneedle array of wet-crosslinked methacrylated hyaluronic acid, Adv. Mater. Technol. 7 (2022), 2100874.
[42] M. Ge, P. Bai, M. Chen, J. Tian, J. Hu, X. Zhi, et al., Utilizing hyaluronic acid as a versatile platform for fluorescence resonance energy transfer-based glucose sensing, Anal. Bioanal. Chem. 410 (2018) 2413–2421.
[43] T. Yao, J. Feng, C. Chu, Z. Ma, H. Han, Cascade controlled release system based on pH-responsive ZIF-8 capsule and enzyme-responsive hyaluronic acid hydrogel for tumor marker detection using electro-readout-mode, Sens. Actuators B: Chem. 348 (2021), 130701.
[44] W. Zhang, X. Li, T. Cui, S. Li, Y. Qian, Y. Yue, et al., PtS2 nanosheets as a peroxidase-mimicking nanozyme for colorimetric determination of hydrogen peroxide and glucose, Microchim. Acta 188 (2021) 1–9.
[45] S. Darvishi, M. Souissi, M. Kharaziha, F. Karimzadeh, R. Sahara, S. Ahadian, Gelatin methacryloyl hydrogel for glucose biosensing using Ni nanoparticles-reduced graphene oxide: an experimental and modeling study, Electrochim. Acta 261 (2018) 275–283.
[46] C. Xu, D. Jiang, Y. Ge, L. Huang, Y. Xiao, X. Ren, et al., A PEDOT: PSS conductive hydrogel incorporated with Prussian blue nanoparticles for wearable and noninvasive monitoring of glucose, Chem. Eng. J. 431 (2022), 134109.
[47] D. Zhai, B. Liu, Y. Shi, L. Pan, Y. Wang, W. Li, et al., Highly sensitive glucose sensor based on Pt nanoparticle/polyaniline hydrogel heterostructures, ACS nano 7 (2013) 3540–3546.
[48] M. Nazari, S. Kashanian, N. Maleki, N. Shahabadi, Laccase immobilized onto graphene oxide nanosheets and electrodeposited gold–cetyltrimethylammonium bromide complex to fabricate a novel catechol biosensor, Bull. Mater. Sci. 42 (2019) 1–10.
[49] A. Nasar, M.M. Rahman, Applications of chitosan (CHI)-reduced graphene oxide (rGO)-polyaniline (PAni) conducting composite electrode for energy generation in glucose biofuel cell, Sci. Rep. 10 (2020) 1–12.
[50] H. Zhu, S. Peng, W. Jiang, Electrochemical properties of PANI as single electrode of electrochemical capacitors in acid electrolytes, Sci. World J. 2013 (2013).
[51] S. Bano, A.S. Ganie, S. Sultana, M.Z. Khan, S. Sabir, The non-enzymatic electrochemical detection of glucose and ammonia using ternary biopolymer based-nanocomposites, N. J. Chem. 45 (2021) 8008–8021.
[52] L.T. Hoa, S.H. Hur, Non-enzymatic glucose sensor based on 3D graphene oxide hydrogel crosslinked by various diamines, J. Nanosci. Nanotechnol. 15 (2015) 8697–8700.
[53] Z. Li, W. Qian, H. Guo, X. Song, H. Yan, R. Jin, et al., Facile preparation of novel Pd nanowire networks on a polyaniline hydrogel for sensitive determination of glucose, Anal. Bioanal. Chem. 412 (2020) 6849–6858.
[54] S.Y. Oh, S.Y. Hong, Y.R. Jeong, J. Yun, H. Park, S.W. Jin, et al., Skin-attachable, stretchable electrochemical sweat sensor for glucose and pH detection, ACS Appl. Mater. Interfaces 10 (2018) 13729–13740.
[55] A. Şavk, K. Cellat, K. Arıkan, F. Tezcan, S.K. Gülbay, S. Kızıldağ, et al., Highly monodisperse Pd-Ni nanoparticles supported on rGO as a rapid, sensitive, reusable and selective enzyme-free glucose sensor, Sci. Rep. 9 (2019) 1–9.
[56] K.G. Sun, S.H. Hur, Highly sensitive non-enzymatic glucose sensor based on Pt nanoparticle decorated graphene oxide hydrogel, Sens. Actuators B: Chem. 210 (2015) 618–623.
[57] M. Waqas, J. Lan, X. Zhang, Y. Fan, P. Zhang, C. Liu, et al., Fabrication of non-enzymatic electrochemical glucose sensor based on Pd− Mn Alloy nanoparticles supported on reduced graphene oxide, Electroanalysis 32 (2020) 1226–1236.
[58] J. Li, Y. Wang, D. Ba, Characterization of semiconductor surface conductivity by using microscopic four-point probe technique, Phys. Procedia 32 (2012) 347–355.
[59] X. Liu, L. Xie, H. Li, Electrochemical biosensor based on reduced graphene oxide and Au nanoparticles entrapped in chitosan/silica sol–gel hybrid membranes for determination of dopamine and uric acid, J. Electro Chem. 682 (2012) 158–163.
[60] M. Yadav, S. Ahmad, Montmorillonite/graphene oxide/chitosan composite: synthesis, characterization and properties, Int J. Biol. Macromol. 79 (2015) 923–933.
[61] L. He, J. Yang, J. Lu, Y. Xiao, Y. Fan, X. Zhang, Preparation and characterization of a novel hyaluronic acid–icariin conjugate hydrogel, Mater. Lett. 136 (2014) 41–44.
[62] A.C. Ferrari, J. Robertson, Interpretation of Raman spectra of disordered and amorphous carbon, Phys. Rev. B 61 (2000) 14095.
[63] F. Tuinstra, J.L. Koenig, Raman spectrum of graphite, J. Chem. Phys. 53 (1970) 1126–1130.
[64] L.J. Cote, F. Kim, J. Huang, Langmuir− Blodgett assembly of graphite oxide single layers, J. Am. Chem. Soc. 131 (2009) 1043–1049.
[65] D. Konios, M.M. Stylianakis, E. Stratakis, E. Kymakis, Dispersion behaviour of graphene oxide and reduced graphene oxide, J. Colloid Interface Sci. 430 (2014) 108–112.
[66] B. Kartick, S.K. Srivastava, I. Srivastava, Green synthesis of graphene, J. Nanosci. Nanotechnol. 13 (2013) 4320–4324.
[67] M. Mm, E. Sa Abo El, H. My, M. Ms, K. Mh, Thermally reduced graphene oxide: synthesis, structural and electrical properties, Int. J. Nanopart. Nanotechnol. 3 (2017).
[68] M. Jahanshahi, A. Morad Rashidi, A. Asghar Ghoreyshi, Synthesis and characterization of thermally-reduced graphene, Iran J. Energy Environ. 4 (2013).
[69] G. Sobon, J. Sotor, J. Jagiello, R. Kozinski, M. Zdrojek, M. Holdynski, et al., Graphene oxide vs. reduced graphene oxide as saturable absorbers for Er-doped passively mode-locked fiber laser, Opt. Express 20 (2012) 19463–19473.
[70] J. Guerrero-Contreras, F. Caballero-Briones, Graphene oxide powders with different oxidation degree, prepared by synthesis variations of the Hummers method, Mater. Chem. Phys. 153 (2015) 209–220.
[71] N. Kumar, V.C. Srivastava, Simple synthesis of large graphene oxide sheets via electrochemical method coupled with oxidation process, ACS Omega 3 (2018) 10233–10242.
[72] N. Kumar, A.K. Srivastava, H.S. Patel, B.K. Gupta, G.D. Varma, Facile synthesis of ZnO–reduced graphene oxide nanocomposites for NO2 gas sensing applications, Eur. J. Inorg. Chem. 2015 (2015) 1912–1923.
[73] K. Kaur, K. Jeet, Electrical conductivity of water-based nanofluids prepared with graphene–carbon nanotube hybrid, Fuller.Nanotub. Carbon Nanostruct. 25 (2017) 726–734.
[74] A. Popov, R. Aukstakojyte, J. Gaidukevic, V. Lisyte, A. Kausaite-Minkstimiene, J. Barkauskas, et al., Reduced graphene oxide and polyaniline nanofibers nanocomposite for the development of an amperometric glucose biosensor, Sensors 21 (2021) 948.
[75] C. Xia, P. Chen, S. Mei, L. Ning, C. Lei, J. Wang, et al., Photo-crosslinked HAMA hydrogel with cordycepin encapsulated chitosan microspheres for osteoarthritis treatment, Oncotarget 8 (2017) 2835.
[76] V.T. Nguyen, N.T. Tran, T.L. Huynh, D.V.H. Le, D. Hoang, Reduced graphene oxide/cellulose microfiber hybrid from the Vietnamese Nipa palm tree: Synthesis, properties, and applications for preparation of poly(methyl methacrylate) composite, J. Thermoplast. Compos Mater. (2021).
[77] M. Ates, M. Yildirim, The synthesis of rGO/RuO2, rGO/PANI, RuO2/PANI and rGO/RuO2/PANI nanocomposites and their supercapacitors, Polym. Bull. 77 (2019) 2285–2307.
[78] M. Kalkan ErdoĞAn, M. SaÇAk, Electromagnetic shielding effectiveness of polyaniline/modified-poly(vinyl alcohol) film composite, Gazi Univ. J. Sci. (2020), 43-33.
[79] I.L. Lera, S. Khasnabis, L.M. Wangatia, F.E. Olu, P.C. Ramamurthy, Insights into the electrochemical behavior and kinetics of NiP@PANI/rGO as a high-performance electrode for alkaline urea oxidation, Electrocatalysis 13 (2022) 283–298.
[80] J. Ma, J. Dai, Y. Duan, J. Zhang, L. Qiang, J. Xue, Fabrication of PANI-TiO2/rGO hybrid composites for enhanced photocatalysis of pollutant removal and hydrogen production, Renew. Energy 156 (2020) 1008–1018.
[81] L. Zhang, M. Wan, Self-assembly of polyaniline—from nanotubes to hollow microspheres, Adv. Funct. Mater. 13 (2003) 815–820.
[82] X. Fu, T. Li, F. Qi, S. Zhang, J. Wen, W. Shu, et al., Designing high electrochemical surface area between polyaniline and hydrogel polymer electrolyte for flexible supercapacitors, Appl. Surf. Sci. 507 (2020), 145135.
[83] C. Xu, S. Guan, S. Wang, W. Gong, T. Liu, X. Ma, et al., Biodegradable and electroconductive poly(3,4-ethylenedioxythiophene)/carboxymethyl chitosan hydrogels for neural tissue engineering, Mater. Sci. Eng. C. Mater. Biol. Appl. 84 (2018) 32–43.
[84] G. Kaur, R. Adhikari, P. Cass, M. Bown, P. Gunatillake, Electrically conductive polymers and composites for biomedical applications, Rsc Adv. 5 (2015) 37553–37567.
[85] D. Kaya, N. Alemdar, Electroconductive hyaluronic acid/gelatin/poly(ethylene oxide) polymeric film reinforced by reduced graphene oxide, J. Appl. Polym. Sci. 136 (2019).

[86] M.U. Celik, S. Ekici, Polyacrylamide-polyaniline composites: the effect of crosslinking on thermal, swelling, porosity, crystallinity, and conductivity properties, Colloid Polym. Sci. 297 (2019) 1331–1343.
[87] S. Das, D.P. Chatterjee, A.K. Nandi, Supramolecular assembly of polythiophene-g-polymethacrylic acid-doped polyaniline with interesting morphological and opto-electronic properties, J. Mater. Chem. A 2 (2014).
[88] J. Li, Y. Xue, A. Wang, S. Tian, Q. Li, S. Bai, Polyaniline functionalized peptide self-assembled conductive hydrogel for 3D cell culture, Gels 8 (2022) 372.
[89] X. Sun, W. Zhong, Z. Zhang, H. Liao, C. Zhang, Stretchable, self-healable and anti-freezing conductive hydrogel based on double network for strain sensors and arrays, J. Mater. Sci. 57 (2022) 12511–12521.
[90] H. Yin, S. Li, H. Xie, Y. Wu, X. Zou, Y. Huang, et al., Construction of polydopamine reduced graphene oxide/sodium carboxymethyl cellulose/polyacrylamide double network conductive hydrogel with high stretchable, pH-sensitive and strain-sensing properties, Colloids Surf. A: Physicochem. Eng. Asp. 642 (2022), 128428.
[91] R. Perveen, A. Nasar, S. Kanchi, H.A. Kashmery, Development of a ternerry condunting composite (PPy/Au/CNT@ Fe3O4) immobilized FRT/GOD bioanode for glucose/oxygen biofuel cell applications, Int J. Hydrog. Energy 46 (2021) 3259–3269.
[92] A. Ray, A. Richter, A. MacDiarmid, A. Epstein, Polyaniline: protonation/deprotonation of amine and imine sites, Synth. Met. 29 (1989) 151–156.
[93] E. Genies, C. Tsintavis, Redox mechanism and electrochemical behaviour or polyaniline deposits, J. Electroanal. Chem. Interfacial Electrochem. 195 (1985) 109–128.
[94] A.J. Heeger, Semiconducting and metallic polymers: the fourth generation of polymeric materials, ACS Publ. (2001) 8475–8491.
[95] S. Ameen, M.S. Akhtar, H.S. Shin, Nanocages-augmented aligned polyaniline nanowires as unique platform for electrochemical non-enzymatic glucose biosensor, Appl. Catal. A: Gen. 517 (2016) 21–29.
[96] Y. Chang, Y. Yao, B. Wang, H. Luo, T. Li, L. Zhi, Reduced graphene oxide mediated SnO2 nanocrystals for enhanced gas-sensing properties, J. Mater. Sci. Technol. 29 (2013) 157–160.
[97] Y.-L.T. Ngo, L. Sui, W. Ahn, J.S. Chung, S.H. Hur, NiMn 2 O 4 spinel binary nanostructure decorated on three-dimensional reduced graphene oxide hydrogel for bifunctional materials in non-enzymatic glucose sensor, Nanoscale 9 (2017) 19318–19327.